Journal of Engineering and Applied Sciences 13 (15): 6293-6302, 2018
ISSN: 1816-949X

Hybrid Chitosan-Silica Nanocomposite Reinforced with Carbon Nanotubes

Mustafa K. Ismael
Department of Mechanical Techniques, Institute of Technology,
Middle Technical University, Baghdad, Iraq

Abstract: This study was conducted to produce Chitosan/MWNTs/SiO_2 (CSMS) nanocomposite powder from aqueous solution through the sol-gel method. The morphology of the CSMS was characterized by Field-Emission Scanning Electron Microscopy (FESEM) X-Ray Diffraction (XRD) Thermogravimetric Analysis (TGA) and Differential Scanning Calorimetry (DSC). The adsorption characteristics were determined by Brunauer-Emmett-Teller (BET) surface area (nitrogen adsorption/desorption isotherms). The results were compared with previously synthesized and characterized Silica Nanoparticles (SiO_2NP). The results showed that CSMS has a 98% adsorption rate which was the largest absorption rate for chitosan by itself. Moreover, the thermal stability of CSMS was demonstrated at temperatures up to 400°C. The pore size of CSMS was determined to be 2.195 nm and the surface area was 478 m^2/g. This study's results indicate that CSMS has novel features that could with stand degradation with efficient adsorption properties.

Key words: Adsorption, biocomposites, chitosan, nanosilica, nanotubes, nanocomposite

INTRODUCTION

Tissue engineering, scaffolding, membranes and fuel cell applications have become ubiquitous in the last 20 years. Polymers and biocomposites have recently been used in many studies to replace traditional materials. Certain scaffolding hydrogel materials have unique mechanical properties. Conventional separation in membrane technology has been demonstrated in several conditions which has led to a reduction in energy conversion (Shaari and Kamarudin, 2015; El-Kadib *et al*., 2010; Albanna *et al*., 2012). In all of these obstacles, chitosan natural polymers have recently been produced with moderate mechanical properties. Additionally, chitosan is ecologically and environmentally friendly, making it broadly applicable in biological applications (Albanna *et al*., 2012). Numerous studies have demonstrated less expensive and more efficient absorbents containing polysaccharides which are based on natural chitosan produced by the deacetylation of chitin (Bailey *et al*., 1999;Wang *et al*., 2009; Kolodynska, 2011, 2012; Budnyak *et al*., 2013; Li *et al*., 2008; Kumar, 2000; Hsien and Rorrer, 1997; Inoue *et al*., 1994). Chitosan shows unique characteristics such as biodegradability combined with biocompatibility, hydrophobicity, nontoxicity, antimicrobial activity and high mechanical strength (Huang *et al*., 2007; Senel and McClure, 2004). However, chitosan has the ability to dissolve in acidic solutions and can sink in alkali solutions because of the degradation of chitosan molecule chains. This degradation leads to weakness in the mechanical properties of chitosan. To overcome this deficiency, several studies using various methods have been conducted such as adding fillers or reinforcements. For example, nanofiller reinforcements such as CNTs, silica, graphene and titanium oxide, enhance chemical crosslinking (Chen *et al*., 2017; Chatterjee *et al*., 2009; Chen *et al*., 2013; Copello *et al*., 2011; Xin *et al*., 2017; El Achaby *et al*., 2014; Cordero-Arias *et al*., 2013).

Nanosilica also has notable properties as a good insulator and other biological activities including drug delivery and biosensing. This carrier material should be bioactive with a high loading/encapsulation rate and an adequate rate of release (Slowing *et al*., 2007, 2008). Various methods have been studied to prepare these hybrid materials based on polysaccharides including chitin and chitosan in many different applications (Zhou *et al*., 2015; Budnyak *et al*., 2014; Ganji and Abdekhodaie, 2008; Kavitha *et al*., 2013; Pabon *et al*., 2004; Puchol *et al*., 2009; Spirk *et al*., 2013). A number of authors have demonstrated using Chitosan-SiO_2 (CSS) (Budnyak *et al*., 2015) in water purification as the adsorbent medium, others have used CSS in a fuel cell proton exchange membrane (Liu *et al*., 2016). The latter has intensively used CSS in drug delivery (Slowing *et al*., 2007, 2008) due its absorption activities and bioactivity characteristics. Carbon Nanotubes (CNTs) have a high surface area with great mechanical properties that have various applications in many disciplines (Coleman *et al*., 2006; Treacy *et al*., 1996; Cadek *et al*., 2002). Chitosan-SiO_2 (CSS) nanocomposites have been

tested successfully for the adsorption of various organic pollution (Tiwari and Dhakate, 2009). It has been reported by Zhang *et al*. (2010) that the anionic surfactant Sodium Dodecyl Sulfate (SDS) leads to a negative charge on CNTs and repulses the silicate anions catalyzed from hydrolysis of TEOS (Zhang *et al*., 2010). Addition of certain protonated 3-Amino Propy Ltriethoxy Silane (APTES) leads to electrostatic attractions (Wu amd Xu, 2009; Che *et al*., 2003). Moreover, Chitosan-MWNT nanocomposites display more affinity for adsorbing CO_2 by impregnation of chitosan (Oslera *et al*., 2017).

The aim of this study was to prepare chitosan/MWNTs/SiO_2 (CSMS) nanocomposite powder with a high surface area and thermal stability which is highly applicable as an ecofriendly compound in water purification or CO_2 fixation. Keeping the surface area as high as possible with a good dispersion of nanoparticles was an ongoing challenge. In order to overcome the lack of bonding due to chitosan degradation or weak cross-linking, MWNTs and SiO_2 nanoparticles were used as reinforcement to successfully circumvent this problem.

MATERIALS AND METHODS

Materials used: Tetraethy lorthosilicate (TEOS), 99.9% purity MW = 208.32, hydrochloric acid MW = 36.5 and concentration 38% ammonium hydroxide concentration 28% assay = 99.99 trace metal (MW = 35.05), methanol (ETOH), MW = 32.04 assay 99.7%, sulfuric acid 95-98% MW = 98.08, nitric acid assay 68.0-70.0%, MW = 63.01 and Tetradecyl Trimethy Lammonium bromide (TTAP), 99%, MW = 336.39 were all purchased from Sigma-Aldrich (Germany). Chitosan powder (CS) or (deacetylated chitin, poly (D-glucosamine)), mesh #80, 99.5% purity was from Suzhu Vitajoy Bio-Tech Co., Ltd., (China), acetic acid (MW = 60.05) analytical reagent was from Chem-Supply Pvt., Ltd, (Australia), Ethanol solution 99.9%, MW = 46.07 was from GCC, (UK) and MWNTs with ID: 2-5 nm, OD: <8 nm, length: 10-30 μm, SSA: >500 m^2/g ASH: <1.5 wt.%, true density: 2.1 g/cm^3 purchased from Hengqiu Graphene Technology Co., Ltd., (China). Finally, Deionized Water (DW) with zero TDS was from a local pharmaceutical company. All chemicals above were reagent grade and used without any further purification or additives.

Chitosan/SiO_2 nanocomposite Synthesis (CSS): In a typical procedure, two mixtures are prepared. The first mixture contained 30 mL of ethanol added to 1 mL of Distilled Water (DW) and 0.5 mL hydrochloric acid. This mixture was later stirred vigorously for 10 min at 250 rpm at room temperature. After stirring was complete, 46.5 mL of Tetraethyl Orthosilicate (TEOS) was added gradually and later stirred for 10 min at 250 rpm. The second mixture contained 0.5 g of Chitosan (CS) powder dissolved in 100 mL of 2% (v/v) acetic acid in a round bottom flask. This mixture was subsequently stirred for 2 h after all of the chitosan had dissolved completely in the diluted acetic acid solution. In order to obtain CSS, the first mixture (sol) of TEOS solution was added dropwise into the second mixture of CS solution using a burette. After the solution was completely poured in the reactant emulation was stirred at 200 rpm for 24 h. Next, the gel was kept for a week for crosslinking and dried in an oven at 60°C. After the gel dried, calcination occurred for 2 h at 500°C. After calcining, the powder was crushed by using an aluminum ball. The mill jar contained a ball-to-powder ratio of 10:1 at 200 rpm and was sieved to ensure that there were no course conglomerates within the powder.

Silica Nanoparticles Synthesis (SiO_2NP): Using a magnetic stirrer at room temperature, 78.7% of TEOS was added to 21.3% methanol by volume and mixed for 10 min at 250 rpm. The previous reactants were added dropwise at a rate of 2 and 5 mL/min to 450 mL of solvent containing 84.4% methanol, 14.7% DW and 0.9% NH_4OH. Again, this mixture was stirred at 200 rpm and heated up to 40°C overnight. After the gel had solidified, it was crushed and calcined for 2 h at 500°C using a muffle furnace.

MWNTs/SiO^2 Synthesis (MS): One hundred milligrams of MWNT was resuspended in 30 g DW for 10 min using a sonication bath. One gram of Tetradecyl Trimethyl-Ammonium bromide (TTAP) was added to the solution (TTAP/MWNTs 10:1 w/w %) and the solution was sonicated again for 1 h using a low power sonicator. The mixture was later added to 80 mL of absolute ETOH and sonicated again for 30 min. A catalyst was added to the above mixture containing 2 mL NH_4OH. In parallel, a solution was prepared by using TEOS:ETOH = 1 mL:40 mL and stirred for 10 min. The solution was subsequently added to the mixture of the MWNTs solution dropwise using a burette and stirred again 24 h and kept at room temperature.

Chitosan/MWNTs/SiO_2 Synthesis (CSMS): In order to obtain CSMS nanocomposites, MWNTs were refluxed in a sulfuric acid and nitric acid mixture ½ (v/v) in order to increase carboxylic and hydroxylic groups as described by Wang *et al*. (2005). One hundred milligrams of MWNTs was added to the solutions and mixed for 12 h at 70°C and later filtered and washed several times and

Fig. 1: Silica and hybrid nanocomposite samples were produced: a) CS-SiO_2,; b) SiO_2 /1; c) SiO_2/2; d) SiO_2-MWNTs and e) CS-MWNTs-SiO_2

finally dried in an oven at 60°C. Silica-chitosan was prepared by dissolving 0.5 g of CS powder in 2% acetic acid with 0.05% functional-MWNTs in an aqueous solution to obtain a ratio of 10: 1 chitosan: MWNTs which was stirred for 2 h. The solution contained 30 mL of ETOH added to 1 mL of DW and 0.5 mL of HCl that was stirred vigorously and poured into the mixture containing 46.5 mL TEOS followed by stirring using a magnetic stirrer for 10 min. The obtained solution was added to the mixture of CS and MWNTs dropwise using a burette and stirred for 24 h. When a gel was formed, the product composite settled over 7 days and was later dried in the oven at 60°C. The hybrid CSMS as a final product is shown in Fig. 1.

Characterization: The thermal measurements were performed using a Differential Scanning Calorimeter (DSC), STA PT-1000 (Linseis Co., Germany). The device was also equipped with Thermal Gravimetric Analysis (TGA) under an atmosphere at 10°C/min. The morphology was observed using a Field Emission Scanning Electron Microscope (FESEM), JEOL, JSM-7000F, (Germany) operated at 15 kV. Also, an AFM AA3000 scanning probe microscope (USA) and a UV-Vis spectrophotometer was used (UV-1800 model, Shimadzu, Japan). The surface area measurement was performed by using BET asAP 2020, Micromeritics, (Instrument Corp., USA) which used nitrogen for adsorption-desorption measurements. X-ray diffraction used Theta-2Theta, a 10-100 scanning range and a scan speed 8°/min, LabX, XRD-6000 (Shimadzu, Japan) with a target Cu-K of = 0.154 nm at 40 kV and 30 mA.

RESULTS AND DISCUSSION

Characterization of SiO_2NP: Prior to investigating the effect of the particle's diameter and surface area on silica nanoparticles, analysis was conducted with AFM, FESEM and BET surface area. This method is in line with the prescribed procedure by Arai *et al.* (2004). Subsequently, two experiments were performed using similar conditions with a variant flow rate of reactant. In Fig. 2a, 2 mL/min was the flow rate of the reactant added. The nanosilica produced tended to be considerably more uniform in size with regular shape while an increasing flow rate of reactant 5 mL/min resulted in a fraction of nanoparticles being aggregated with a blocky shape as shownin Fig. 2b. The BET surface area confirmed that the flow rate of reactant effects the particle size and a 2 mL/min flow rate of reactant had a 200.52 m^2/g surface area which was decreased (180.22 m^2/g) when reactant was poured at a 5 mL/min flow rate. The size of the nanoparticles was measured by using AFM as shown in Fig. 3. In Fig. 3a-b and the average diameter was 79.09 nm. For the 5 mL/min flow rate, the average particle size diameter was 68.33 nm as shown in Fig. 3c-d.

Characterization of CSS nanocomposite: The CSS nanocomposite was synthesized by the formation of an inorganic network in an organic polymer using sol-gel methodologies Budnyak *et al.* (2015) found an amine group of chitosan was protonated to form NH_3+ ion in acidic conditions. This finding means that alkoxysilane is not only covalently bound to chitosan but is also incorporated into the matrix. In this research, the hybrid composite material exhibited significantly strange chemical bonding between the two covenant ionic organics and the inorganic media. The hydroxyl groups may form hydrogen bonds or be immersed with the condensation reaction by silanol groups to form a hydrolysis precursor which later promotes silica molecule nucleation (Chassary *et al.*, 2004). The amino group in the

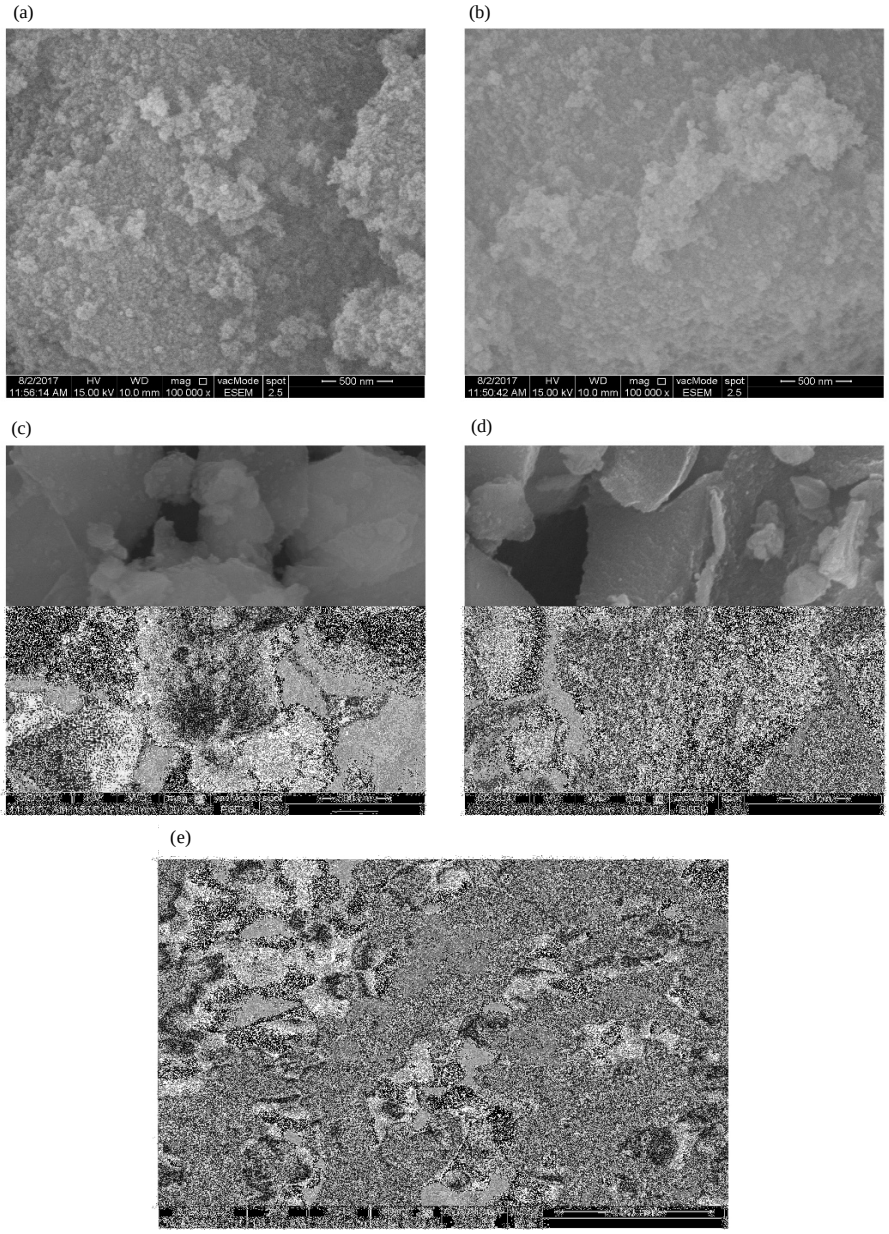

Fig. 2: FESEM micrographs of: a) Silica/1; b) Silica/2; c) CS-SiO_2 nano-powder; d) CS-MWNTs-SiO_2 nanocomposite and e) MWNTs deposited with nanosilica particles

chitosan molecules expedited the hydrolysis of TEOS condensation to create silanol groups from silicas with a group of carbonyls in polymer to form Si-O-C bonds. In Fig. 2c, the final product of the silica-chitosan nanocomposite after ball milling processes had a rough and irregular shape and flake layer due to the crushing forces.

Characterization of MS nanocomposite: The bonding technique was completely different between silica and MWNTs. Silica itself cannot be deposited on MWNTs because of the repulsive negative charge of the hydrolysis TEOS to form Si-O-C linkage and functional groups. Though some of the saline bonded with the hydrogen-bond interaction of MWNTs, it was not sufficient to cover all of the tube as confirmed by Liu *et al.* (2016). Mixing the CNT suspension with cationic TTAB promoted a positive-charged attraction of saline from hydrolysis of TEOS. Figure 2e shows the MWNTs after the silica was deposited on MWNTs. It can

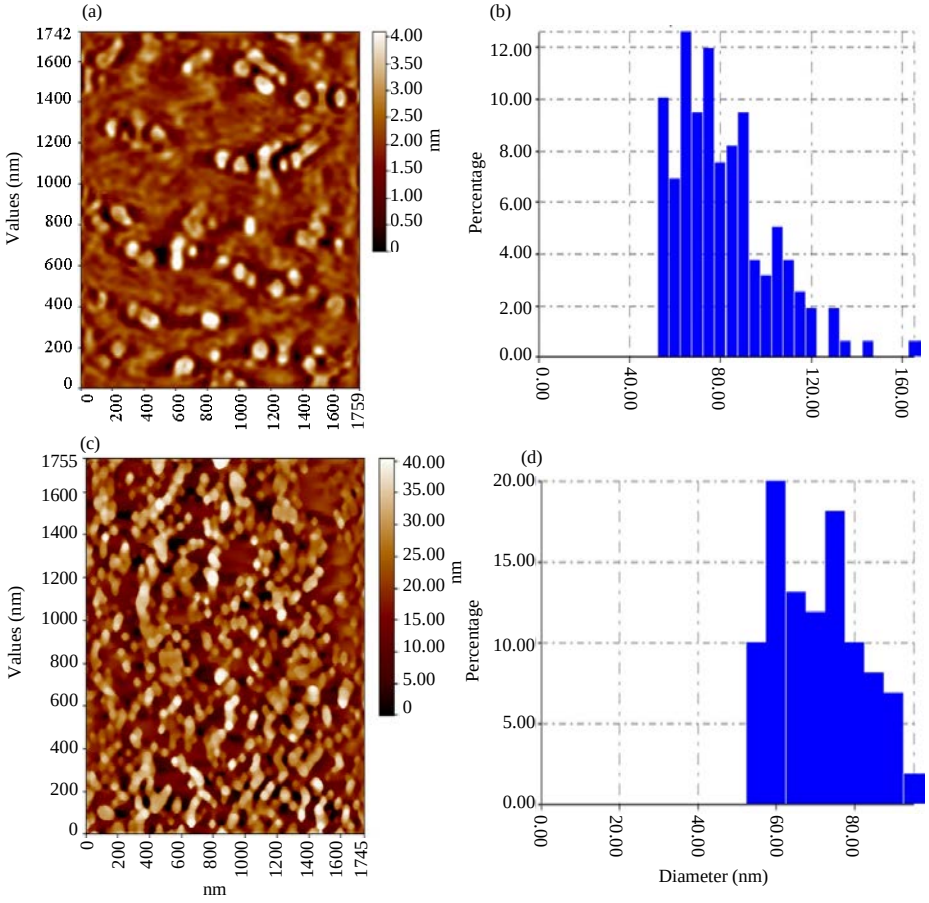

Fig. 3: a) AFM results of silica-NP; b) image of silica/1; c) GCD for graph and d) Image of silica/2 and GCD 0 for graph

be seen clearly that a uniform coating of SiO_2 on MWNTs increased the tube diameter from <8 nm to the average diameter of 70 nm.

Characterization of CSMS nanocomposite: In order to choose a useful route for making appropriate hybrid CSMS nanocomposites via sol-gel methods, the functional groups of MWNTs are used as an anchoring bonding between chitosan and hydroxylic, carboxylic groups on one side and silica with chitosan by hydrogen bonds on the other. The overall bonding very weak in this case, using hybridized composite materials, the surfactant was omitted by existing hydroxyl and carboxylic groups. The results were bonded CSMS. This mechanism is explained in the hypothesis scheme in Fig. 4. The FESEM image in Fig. 2d shows the hybrid CSMS powder after the ball milling process and the resulting sharp cleavage with a very uniform dimple outside the skins, referred to as MWNTs tips.

When XRD for CSMS analysis was compared with silica as base materials, the X-ray spectrum as shown in Fig. 5, from all samples represented a similar pattern that was based on amorphous silica according to the ICDD number (00-050-1432) for silicon oxide. This finding indicates that silica-based nanocomposite are dominant and other elements such as MWNTs are fully coated with silica nanoparticles. The main peak in the 2 was 20.72° which had a brooding shape, especially in the MS and silica/1 and silica/2, revealing the nanoparticles of silica.

DSC and TGA were used to study the thermal stability and decomposition of hybrid nanocomposites. The DSC of MS is shown in Fig. 6a. Two exotherms occur where the average onset temperature was 85.2°C and 577.9°C, respectively. The first of these was the evaporation of water in silica pores over CNTs as confirmed by Bjornstrom *et al*. (2004) and similar to a phenomenon seen in silica, CSS and CSMS nanocomposites, shown in Fig. 6b. The other exotherm at 577.9°C represented a carbon decomposition when evaporation began. The endo-exotherm line between 85.2°Cand 577.9°C refers to the decomposition layers of silica coated by MWNTs. There were slight differences in the exotherm peaks of CSS and CSMS with high enthalpy -422 and -509 J/g, respectively.

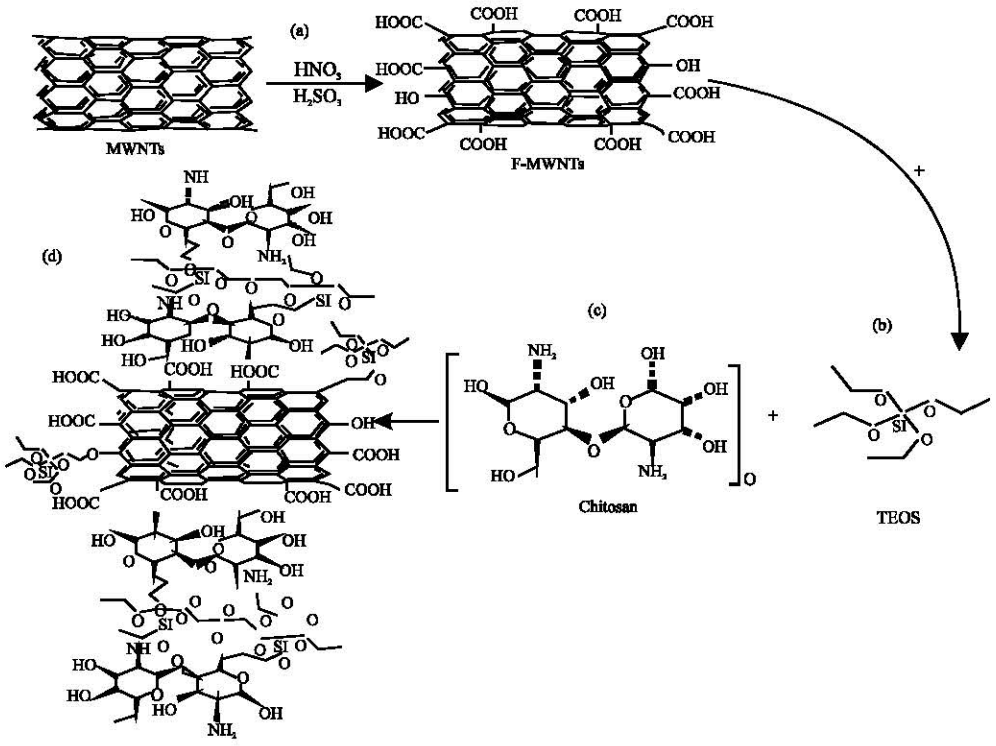

Fig. 4a-c): The proposed scheme of chitosan-silica-MWNTs composite bonding

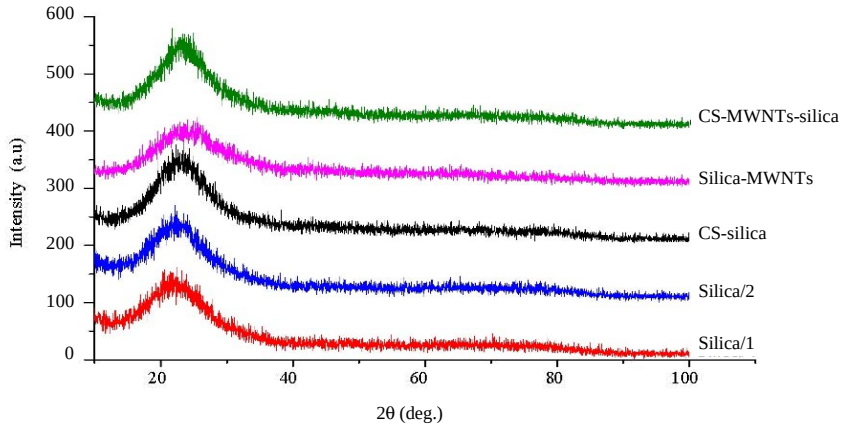

Fig. 5: XRD pattern of silica, CS-silica, silica-MWNTs and CS-MWNTs-silica

Thus, the exotherm was due to a large amount of heat being liberated during the evaporation of water from chitosan. However, the nanocomposite of CSMS tended to be more stable at 500°C before it started to degrade compared to other silica nanoparticles and CS-silica. In Fig. 6c, the TGA-curves of silica, CSS, MS and CSMS nanocomposite shows that in the temperature range between 100 to 700°C, the weight loss of MS was approximately 10% between 445-690°C and increased by approximately 20% between 690-700°C. Silica itself had no significant change, changing only approximately 2-4%. CSMS weight loss was 8% between 440-690°C and 20% between 690-700°C. Nanocomposite CSMS lost more compared with chitosan itself, displaying approximately 35 and 50% weight loss, respectively. The nitrogen adsorption isotherm vs. relative pressure (P/Po) of the plot and 1/[Q(P/Po-1)] vs. relative pressure (P/Po) are shown in Fig. 7a, b, respectively. The isotherm patterns represent high-quantity adsorption for CSMS followed CSS, silica and MS. Subsequently, chitosan had a lower

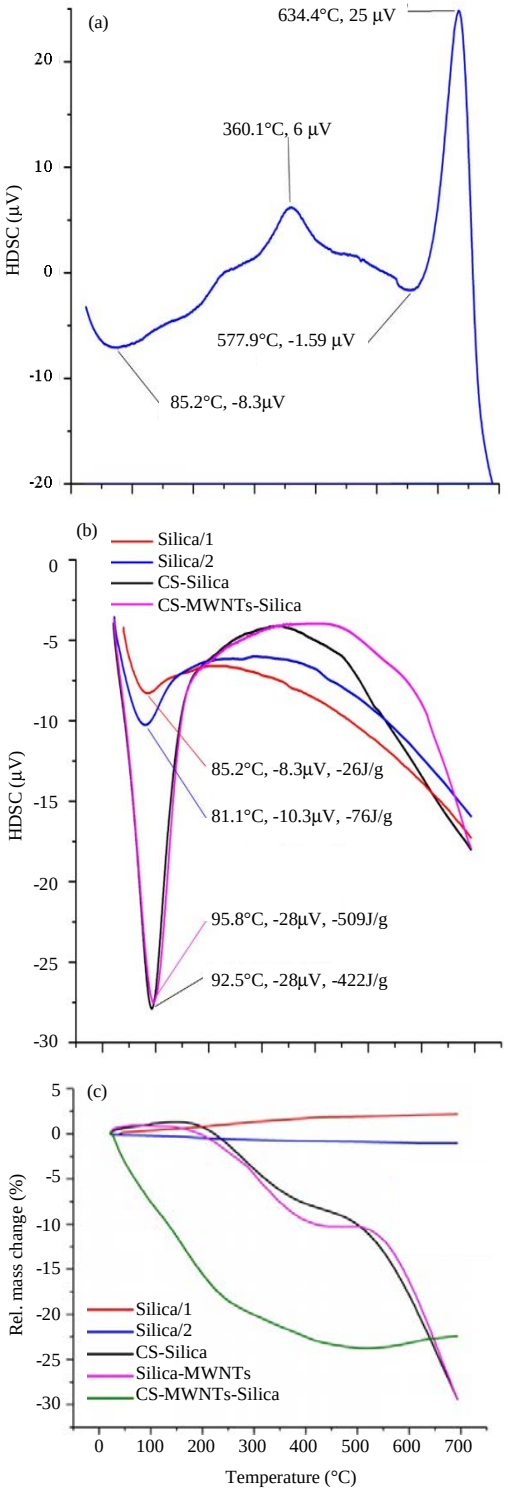

Fig. 6: Thermal analysis of hybrid chitosan: a) DSC of MWNTs/SiO_2 film; b) DSC of CS-SiO_2;m and c) TGA-curves of SiO_2-NP and hybrid CS-SiO_2-MWNTs nanocomposite

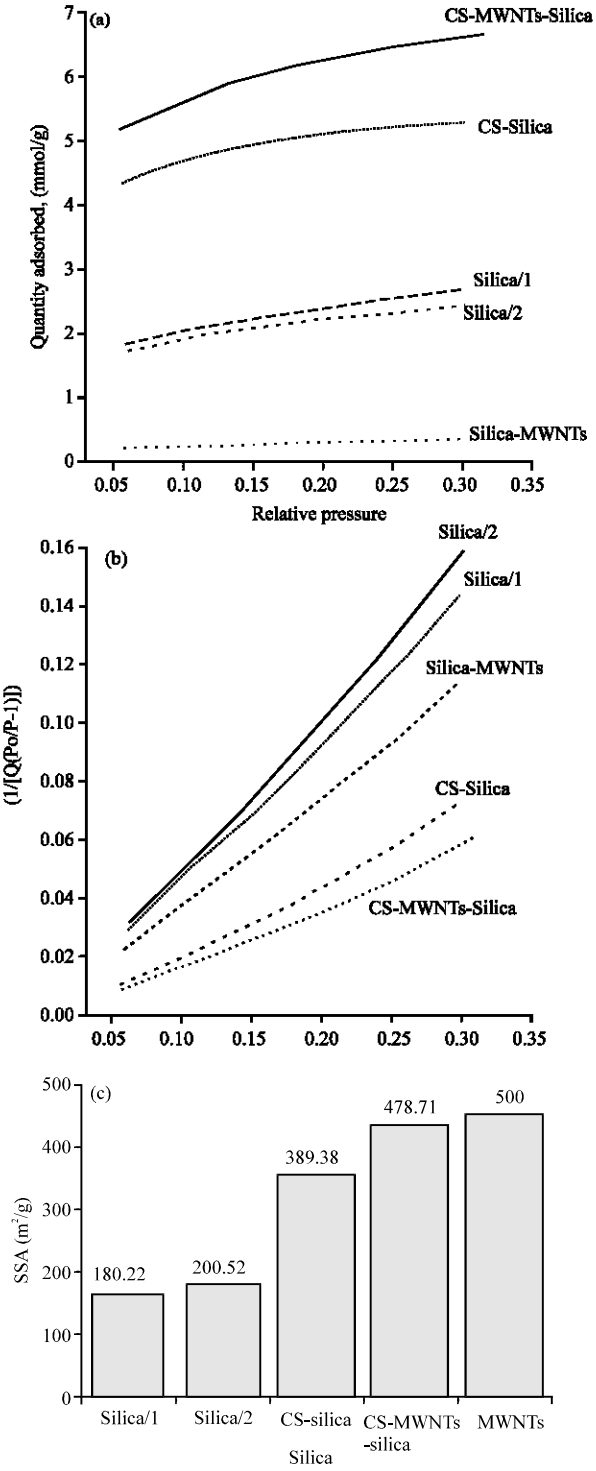

Fig. 7: Adsorption plot of SiO_2-NP and hybrid CS-SiO_2-MWNTs nanocomposite obtained at 200°C for 6hrs: a) N_2 adsorption isotherm vs. (P/Po); b) 1/[Q(P/Po-1)] vs. (P/Po); c) bar chart of SiO_2-NP-CS-MWNTs nanocomposite

Table 1: Hybrid chitosan/silica/MWNTs nanocomposite surface area and pores volume and size

Hybrid chitosan/silica	BET (m^2/g)	Pore volume (cm^3/g)	Pore size (nm)
CS-MWNTs-silica	478.7	0.2620	2.1950
CS-silica	389.3	0.2080	2.1420
Silica/2	200.5	0.9950	19.8.58
Silica/1	180.2	0.8920	19.8070
Silica-MWNTs	24.4	0.0702	11.0660

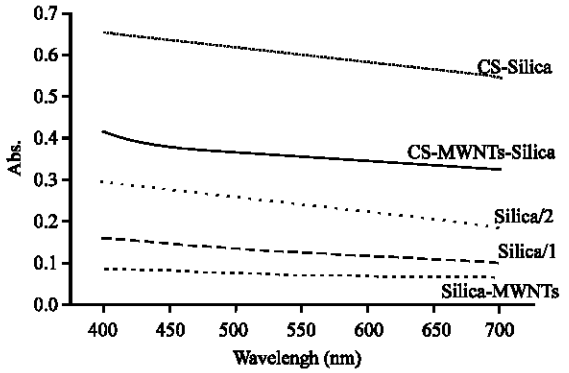

Fig. 8: UV-vis spectra for nanocomposite materials based on silica and chitosan

specific surface area reported between 4.5-7.4 m^2/g (Moosa *et al*., 2016; Alkhamis *et al*., 2008). The high surface area of CSMS was due to a large surface area of silica and MWNTs while the smaller surface area of MS was attributable to the TTAP which may cause endohedral functionalization of MWNTs with exohedral functional groups and pore size and pore volume were kept small in CSMS (Table 1). Thus, there is an adverse effect on the overall final product. Figure 7c shows a comparison of adsorption capacity of CSMS, CSS, MS and SiO_2NP. UV-vis spectra for nanocomposite chitosan is shown in Fig. 8. The absorption was proportional to the concentration of CS in silica and MWNTs. However, CSMS had medium absorption in ethanol solutions. According to Lambert–Beer's law, the absorbance increase within dispersed MWNTs was confirmed by Sobolkina *et al*. (2012). The well-dispersed MWNTs in CS with silica have higher absorption than MS.

CONCLUSION

The 0.05% MWNTs with TEOS was selected to compound with chitosan via sol-gel methods to prepare a hydrogel hybrid nanocomposite in order to improve the adsorption and thermal stability of composites which are capable of being used in many aggressive media. Nitrogen adsorption isotherm and 1/[Q(P/Po-1)] vs. relative pressure showed that CSMS had a high adsorption quantity, improving the absorption by 98%. Additionally, thermal stability was up to 400°C. SiO_2NP with MWNTs had an excellent effect on chitosan through the reinforcement effect as well as thermal stability TGA-SiO_2NP (between 60-70 nm) showed high stability in the range of 100-700°C. XRD of hybrid CSMS nanocomposites showed a predominant amorphous nanosilica peak as well as MWNTs itself which were fully coated with SiO_2NP. MWNTs coated with SiO_2NP using TTAB promoted the positive-charged attraction between MWNTs and saline from hydrolysis TEOS. The results were a 70% increase in tube thickness but adverse effects led to a reduced surface area. To resolve this defect, functional groups on the outer layer of MWNTs instead of endohedral functionalization were promoted. FESEM revealed that SiO_2NP facilitated this effect which was confirmed by AFM. FESEM observation of MS revealed that MWNTs diameter increased indicating the silica-coated tubes and the UV-vis spectra for hybrid CSMS nanocomposites showed the combination of MWNTs with CSS had a 0.3-0.4 absorbance in the 400-700 nm wavelength range. This absorbance was higher than that observed with SiO_2NP and MS alone but lower than that observed with CSS. These attributes increased the absorption by a distribution of MWNTs in the whole composite.

ACKNOWLEDGEMENT

I would like to thank the staff and employers in the Oil Ministry-Petroleum Research and Development Center for providing valuable feedback and support for this study.

REFERENCES

Albanna, M.Z., T.H. Bou-Akl, H.L. Walters III and H.W. Matthew, 2012. Improving the mechanical properties of chitosan-based heart valve scaffolds using chitosan fibers. J. Mech. Behav. Biomed. Mater., 5: 171-180.

Alkhamis, K.A., M.S. Salem and M.S. Khanfar, 2008. The sorption of ketotifen fumarate by chitosan. Aaps Pharm. Sci. Tech., 9: 866-869.

Arai, Y., H. Segawa and K. Yoshida, 2004. Synthesis of nano silica particles for polishing prepared by sol-gel method. J. Sol Gel Sci. Technol., 32: 79-83.

Bailey, S.E., T.J. Olin, R.M. Bricka and D.D. Adrian, 1999. A review of potentially low-cost sorbents for heavy metals. Water Res., 33: 2469-2479.

Bjornstrom, J., A. Martinelli, A. Matic, L. Borjesson and I. Panas , 2004. Accelerating effects of colloidal nano-silica for beneficial calcium-silicate-hydrate formation in cement. Chem. Phys. Lett., 392: 242-248.

Budnyak, T.M., I.V. Pylypchuk, V.A. Tertykh, E.S. Yanovska and D. Kolodynska, 2015. Synthesis and adsorption properties of chitosan-silica nanocomposite prepared by sol-gel method. Nanoscale Res. Lett., 10: 87-96.

Budnyak, T.M., V.A. Tertykh and E.S. Yanovska, 2013. Chitosan and its derivatives as sorbents for effective removal of metal ions. Surf., 5: 118-134.

Budnyak, T.M., V.A. Tertykh and E.S. Yanovska, 2014. Chitosan immobilized on saponite surface in extraction of V(V), Mo(VI) and Cr(VI) Oxoanions. Chem. Phys. Surf. Technol., 5: 445-453.

Cadek, M., J.N. Coleman, V. Barron, K. Hedicke and W.J. Blau, 2002. Morphological and mechanical properties of carbon-nanotube-reinforced semicrystalline and amorphous polymer composites. Appl. Phys. Lett., 81: 5123-5125.

Chassary, P., T. Vincent and E. Guibal, 2004. Metal anion sorption on chitosan and derivative materials: A strategy for polymer modification and optimum use. React. Funct. Polym., 60: 137-149.

Chatterjee, S., M.W. Lee and S.H. Woo, 2009. Enhanced mechanical strength of chitosan hydrogel beads by impregnation with carbon nanotubes. Carbon, 47: 2933-2936.

Che, S., A.E. Garcia-Bennett, T. Yokoi, K. Sakamoto and H. Kunieda *et al*., 2003. A novel anionic surfactant templating route for synthesizing mesoporous silica with unique structure. Nature Mater., 2: 801-805.

Chen, J., X. Shi, Y. Zhan, X. Qiu and Y. Du *et al*., 2017. Construction of horizontal stratum landform-like composite foams and their methyl orange adsorption capacity. Appl. Surf. Sci., 397: 133-143.

Chen, Y., L. Chen, H. Bai and L. Li, 2013. Graphene oxide-chitosan composite hydrogels as broad-spectrum adsorbents for water purification. J. Mater. Chem. A, 1: 1992-2001.

Coleman, J.N., U. Khan, W.J. Blau and Y.K. Gun'ko, 2006. Small but strong: A review of the mechanical properties of carbon nanotube-polymer composites. Carbon, 44: 1624-1652.

Copello, G.J., A.M. Mebert, M. Raineri, M.P. Pesenti and L.E. Diaz, 2011. Removal of dyes from water using chitosan hydrogel/SiO_2 and chitin hydrogel/SiO_2 hybrid materials obtained by the sol-gel method. J. Hazard. Mater., 186: 932-939.

Cordero-Arias, L., S. Cabanas-Polo, H. Gao, J. Gilabert and E. Sanchez *et al*., 2013. Electrophoretic deposition of nanostructured-TiO_2/chitosan composite coatings on stainless steel. RSC. Adv., 3: 11247-11254.

El Achaby, M., Y. Essamlali, N. El Miri, A. Snik and K. Abdelouahdi *et al*., 2014. Graphene oxide reinforced chitosan/polyvinylpyrrolidone polymer bio-nanocomposites. J. Appl. Polym. Sci., 131: 1-11.

El-Kadib, A., K. Molvinger, M. Bousmina and D. Brunel, 2010. Decoration of Chitosan microspheres with inorganic oxide clusters: Rational design of hierarchically porous, stable and cooperative acid-base nanoreactors. J. Catal., 273: 147-155.

Ganji, F. and M.J. Abdekhodaie, 2008. Synthesis and characterization of a new thermosensitive chitosan-PEG diblock copolymer. Carbohydr. Polym., 74: 435-441.

Hsien , T.Y. and G.L. Rorrer, 1997. Heterogeneous cross-linking of chitosan gel beads: Kinetics, modeling and influence on cadmium ion adsorption capacity. Ind. Eng. Chem. Res., 36: 3631-3638.

Huang, X.J., D. Ge and Z.K. Xu, 2007. Preparation and characterization of stable chitosan nanofibrous membrane for lipase immobilization. Eur. Polym. J., 43: 3710-3718.

Inoue, K., K. Yoshizuka and Y. Baba, 1994. Adsorption of Metal Ions on Chitosan and Chemically Modified Chitosan and their Application to Hydrometallurgy. In: Biotechnology and Bioactive Polymers, Gebelein, C.G. and C.E. Carraher (Eds.). Springer, Boston, Massachusetts, ISBN: 978-1-4757- 9521-9, pp: 35-41.

Kavitha, K., S. Sutha, M. Prabhu, V. Rajendran and T. Jayakumar, 2013. $_{In\ situ}$ synthesized novel biocompatible titania-chitosan nanocomposites with high surface area and antibacterial activity. Carbohydr. Polym., 93: 731-739.

Kolodynska, D., 2011. Chitosan as an effective low-cost sorbent of heavy metal complexes with the polyaspartic acid. Chem. Eng. J., 173: 520-529.

Kolodynska, D., 2012. Adsorption characteristics of chitosan modified by chelating agents of a new generation. Chem. Eng. J., 179: 33-43.

Kumar, M.N.V.R., 2000. A review of chitin and chitosan applications. React. Funct. Polym., 46: 1-27.

Li, C.B., S. Hein and K. Wang, 2008. Biosorption of chitin and chitosan. Mater. Sci. Technol., 24: 1088-1099.

Liu, H., C. Gong, J. Wang, X. Liu and H. Liu *et al*., 2016. Chitosan/silica coated carbon nanotubes composite proton exchange membranes for fuel cell applications. Carbohydr. Polym., 136: 1379-1385.

Moosa, A.A., A.M. Ridha and N.A. Kadim, 2016. Use of biopolymer adsorbent in the removal of phenol from aqueous solution. Am. J. Mater. Sci., 6: 95-104.

Osler, K., N. Twala, O.O. Oluwasina and M.O. Daramola, 2017. Synthesis and performance evaluation of Chitosan/Carbon nanotube (Chitosan/MWCNT) composite adsorbent for post-combustion carbon dioxide capture. Energy Procedia, 114: 2330-2335.

Pabon , E., J. Retuert, R. Quijada and A. Zarate, 2004. TiO_2-SiO_2 mixed oxides prepared by a combined sol-gel and polymer inclusion method. Microporous Mesoporous Mater., 67: 195-203.

Puchol, V., J. El-Haskouri, J. Latorre, C. Guillem and A. Beltran *et al*., 2009. Biomimetic chitosan-mediated synthesis in heterogeneous phase of bulk and mesoporous silica nanoparticles. Chem. Commun., 19: 2694-2696.

Senel, S. and S.J. McClure, 2004. Potential applications of chitosan in veterinary medicine. Adv. Drug Deliv. Rev., 56: 1467-1480.

Shaari, N. and S.K. Kamarudin, 2015. Chitosan and alginate types of bio-membrane in fuel cell application: An overview. J. Power Sources, 289: 71-80.

Slowing, I.I., B.G. Trewyn, S. Giri and V.S.Y. Lin, 2007. Mesoporous silica nanoparticles for drug delivery and biosensing applications. Adv. Funct. Mater., 17: 1225-1236.

Slowing, I.I., J.L. Vivero-Escoto, C.W. Wu and V.S.Y. Lin, 2008. Mesoporous silica nanoparticles as controlled release drug delivery and gene transfection carriers. Adv. Drug Delivery Rev., 60: 1278-1288.

Sobolkina, A., V. Mechtcherine, V. Khavrus, D. Maier and M. Mende *et al*., 2012. Dispersion of carbon nanotubes and its influence on the mechanical properties of the cement matrix. Cem. Concr. Compos., 34: 1104-1113.

Spirk, S., G. Findenig, A. Doliska, V.E. Reichel, N.L. Swanson and *et al*., 2013. Chitosan-silane sol-gel hybrid thin films with controllable layer thickness and morphology. Carbohydr. Polym., 93: 285-290.

Tiwari, A. and S.R. Dhakate, 2009. Chitosan-SiO_2-multiwall carbon nanotubes nanocomposite: A novel matrix for the immobilization of creatine amidinohydrolase. Intl. J. Biol. Macromol., 44: 408-412.

Treacy, M.M.J., T.W. Ebbesen and J.M. Gibson, 1996. Exceptionally high Young's modulus observed for individual carbon nanotubes. Nature, 381: 678-680.

Wang, M., L. Xu, J. Peng, M. Zhai and J. Li *et al*., 2009. Adsorption and desorption of Sr(II) ions in the gels based on polysaccharide derivates. J. Hazard. Mater., 171: 820-826.

Wang, S.F., L. Shen, W.D. Zhang and Y.J. Tong, 2005. Preparation and mechanical properties of chitosan/carbon nanotubes composites. Biomacromolecules, 6: 3067-3072.

Wu, X.J. and D. Xu, 2009. Formation of yolk/SiO_2 shell structures using surfactant mixtures as template. J. Am. Chem. Soc., 131: 2774-2775.

Xin, S., Z. Zeng, X . Zhou, W. Luo and X. Shi *et al*., 2017. Recyclable Saccharomyces cerevisiae loaded nanofibrous mats with sandwich structure constructing via. bio-electrospraying for heavy metal removal. J. Hazard. Mater., 324: 365-372.

Zhang, M., X. Zhang, X. He, L. Chen and Y. Zhang, 2010. A facile method to coat mesoporous silica layer on carbon nanotubes by anionic surfactant. Mater. Lett., 64: 1383-1386.

Zhou, H.Y., L.J. Jiang, P.P. Cao, J.B. Li and X.G. Chen, 2015. Glycerophosphate-based chitosan thermosensitive hydrogels and their biomedical applications. Carbohydr. Polym., 117:524-536.